



HAL
open science

Gradients of Rac1 Nanoclusters Support Spatial Patterns of Rac1 Signaling

Amanda Remorino, Simon de Beco, Fanny Cayrac, Fahima Di Federico, Gaetan Cornilleau, Alexis Gautreau, Maria Carla Parrini, Jean-Baptiste Masson, Maxime Dahan, Mathieu Coppey

► **To cite this version:**

Amanda Remorino, Simon de Beco, Fanny Cayrac, Fahima Di Federico, Gaetan Cornilleau, et al.. Gradients of Rac1 Nanoclusters Support Spatial Patterns of Rac1 Signaling. *Cell Reports*, 2017, 21 (7), pp.1922-1935. 10.1016/j.celrep.2017.10.069 . hal-01637091

HAL Id: hal-01637091

<https://hal.sorbonne-universite.fr/hal-01637091>

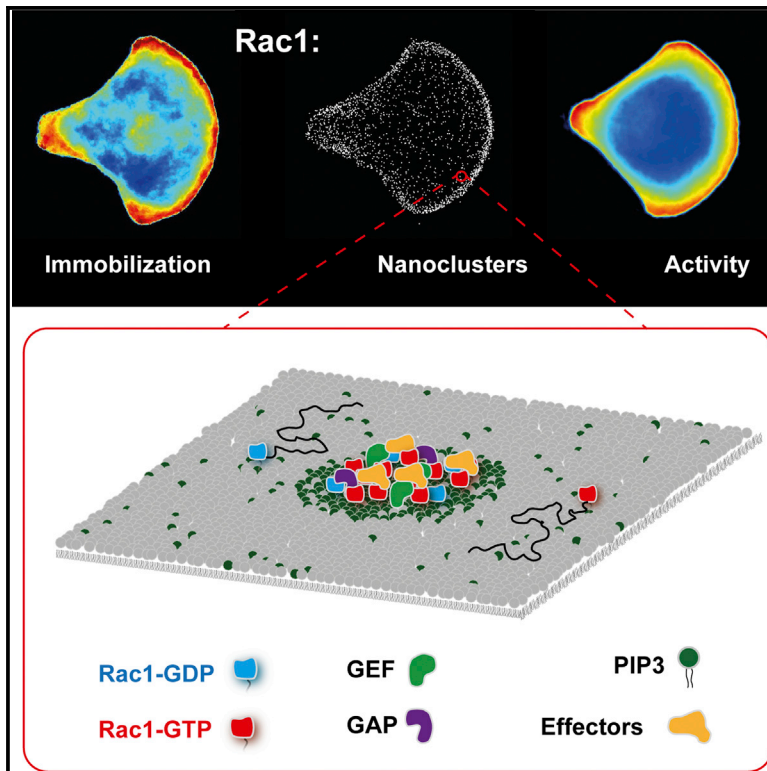
Submitted on 17 Nov 2017

HAL is a multi-disciplinary open access archive for the deposit and dissemination of scientific research documents, whether they are published or not. The documents may come from teaching and research institutions in France or abroad, or from public or private research centers.

L'archive ouverte pluridisciplinaire **HAL**, est destinée au dépôt et à la diffusion de documents scientifiques de niveau recherche, publiés ou non, émanant des établissements d'enseignement et de recherche français ou étrangers, des laboratoires publics ou privés.

Gradients of Rac1 Nanoclusters Support Spatial Patterns of Rac1 Signaling

Graphical Abstract



Authors

Amanda Remorino, Simon De Beco, Fanny Cayrac, ..., Jean-Baptiste Masson, Maxime Dahan, Mathieu Coppey

Correspondence

mathieu.coppey@curie.fr

In Brief

Rac1 is a small GTPase protein controlling the polymerization of actin at the front of migrating cells. Using super-resolution microscopy, Remorino et al. show that Rac1 forms nanoclusters of heterogeneous composition, which presumably act as discrete signaling platforms. The subcellular distribution of Rac1 nanoclusters follows its pattern of activation.

Highlights

- 20% of membrane-bound Rac1 forms immobile nanoclusters of ~50–100 molecules
- Nanoclusters are formed thanks to Rac1 polybasic tail and PIP2/PIP3 charged lipids
- Interaction of Rac1 with GEF/GAP/effector partners enriches nanoclusters locally
- The distribution of Rac1 nanoclusters follows the pattern of Rac1 activity



Gradients of Rac1 Nanoclusters Support Spatial Patterns of Rac1 Signaling

Amanda Remorino,¹ Simon De Beco,¹ Fanny Cayrac,¹ Fahima Di Federico,¹ Gaetan Cornilleau,¹ Alexis Gautreau,² Maria Carla Parrini,³ Jean-Baptiste Masson,^{4,5} Maxime Dahan,¹ and Mathieu Coppey^{1,6,*}

¹Laboratoire Physico-Chimie, Institut Curie, CNRS UMR168, Paris-Science Lettres, Université Pierre et Marie Curie-Paris 6, 75005 Paris, France

²Ecole Polytechnique, Université Paris-Saclay, CNRS UMR7654, 91120 Palaiseau, France

³Institut Curie, Centre de Recherche, Paris Sciences Lettres, ART Group, Inserm U830, Paris 75005, France

⁴Decision and Bayesian Computation, Institut Pasteur, 25 Rue du Docteur Roux, Paris, 75015, France

⁵Bioinformatics and Biostatistics Hub - C3BI, USR 3756 IP CNRS, Paris, France

⁶Lead Contact

*Correspondence: mathieu.coppey@curie.fr

<https://doi.org/10.1016/j.celrep.2017.10.069>

SUMMARY

Rac1 is a small RhoGTPase switch that orchestrates actin branching in space and time and protrusion/retraction cycles of the lamellipodia at the cell front during mesenchymal migration. Biosensor imaging has revealed a graded concentration of active GTP-loaded Rac1 in protruding regions of the cell. Here, using single-molecule imaging and super-resolution microscopy, we show an additional supramolecular organization of Rac1. We find that Rac1 partitions and is immobilized into nanoclusters of 50–100 molecules each. These nanoclusters assemble because of the interaction of the polybasic tail of Rac1 with the phosphoinositide lipids PIP2 and PIP3. The additional interactions with GEFs and possibly GAPs, downstream effectors, and other partners are responsible for an enrichment of Rac1 nanoclusters in protruding regions of the cell. Our results show that subcellular patterns of Rac1 activity are supported by gradients of signaling nanodomains of heterogeneous molecular composition, which presumably act as discrete signaling platforms.

INTRODUCTION

Cell migration and tissue invasion have important roles in cancer metastasis and embryonic development. Among the different mechanisms of migration, protrusion-based mesenchymal migration involves the formation of structures called lamellipodia that alternate between protruding and retracting cycles through actin polymerization and depolymerization (Krause and Gautreau, 2014). The regulation of this highly dynamic and adaptable mechanism of motion dictates the outcomes of many cellular processes. For example, the stiffness of the branched actin network (Bieling et al., 2016), the frequency of its oscillations (Mendoza et al., 2015), the relative ratio of elongation and branching (Bisi et al., 2013), and membrane trafficking (Gautier et al., 2011) can be tuned to yield

distinct phenotypic effects. This regulation is achieved through a complex coordination of many signaling pathways in which RhoGTPases, small molecular switches that integrate multiple inputs to orchestrate the dynamics of the cytoskeleton, play a pivotal role.

One of the most studied RhoGTPases, Rac1, is at the core of signaling pathways regulating cell polarization and migration. Rac1 is activated and deactivated at the plasma membrane, and possibly at endomembranes, through the interaction with guanine nucleotide exchange factors (GEFs) and GTPase-activating proteins (GAPs), respectively. Rac1 shuttles to and from the plasma membrane through its interaction with Rho GDP-dissociation inhibitors (GDIs), which mask its prenyl group. Rac1 presents spatiotemporal patterns of activity (Pertz, 2010; Machacek et al., 2009) that extend over a few micrometers and last for a few minutes during cell migration (Fritz and Pertz, 2016). Localized shuttling of Rac1 by GDIs and localized activation by GEFs are two mechanisms capable of producing and maintaining activation profiles. They represent different layers of regulation, and their relative importance is still not clear (Woods et al., 2015; Hodgson et al., 2016).

Modeling studies (Bement et al., 2006) have identified three main variables controlling the spatiotemporal properties of its subcellular gradients of activation: the spatial distribution of activators and deactivators (GEFs and GAPs, respectively), the cycling rates between activation states, and the diffusivity of RhoGTPases at the membrane. Assuming a sharply localized GEF and a uniform GAP distribution, the spatial extent of active Rac1 simply depends on its lifetime in the GTP-bound state and its lateral diffusion coefficient. Yet we do not know whether the spatial extent of Rac1 activity gradients in the cell, generated by a specific distribution of activators and deactivators, is maintained because of low mobility or short lifetimes. Some of the mechanisms that localize GEFs and GAPs have been identified and described (reviewed by Fritz and Pertz, 2016). Lipid-interaction domains with varying lipid specificity, BAR domains, tyrosine kinases, scaffold proteins, adhesion complexes, and the cytoskeleton have been shown to selectively direct GEFs and GAPs to different plasma membrane (PM) subdomains. In contrast, only a few works have focused on the study of RhoGTPases diffusivities (Shibata et al., 2013; Chazeau et al.,

2014; Das et al., 2015) or on the determination of cycling rates (Parrini et al., 2011; Davis et al., 2013).

In addition to the molecular parameters encoding the cellular-scale patterns of Rac1 activity, there might be a supramolecular organization of Rac1 signaling not accessible by conventional microscopy. In the past decade, several studies have reported the existence of nanoclusters for membrane-bound signaling proteins (Bonny et al., 2016). It has been argued that all signaling proteins might be regulated through nanoclusters (Garcia-Parajo et al., 2014). These nanoclusters accumulate around ten proteins in less than 250 nm² areas (Wittinghofer, 2014), producing highly localized increase of concentrations that allow putative thresholds to be overcome. As such, their assumed function is to ensure the transduction of signals with high fidelity, each nanocluster acting as discrete signal processing units digitalizing the input (Harding and Hancock, 2008). The small G protein Ras presents the best-studied case of nanoclustering (Wittinghofer, 2014). On the plasma membrane, about 44% of Ras proteins are organized into ~9 nm nanoclusters composed of four to seven proteins and having a 0.1–1 s lifetime (Hancock and Parton, 2005). Active and inactive forms of Ras are segregated into different nanoclusters. Ras proteins exist in different isoforms: H-Ras, N-Ras, and K-Ras. They differ in their lipid anchors and yield nanoclusters of varying acidic phospholipid, cholesterol, and scaffold protein composition. As a consequence, they behave differently when the plasma membrane is perturbed through cholesterol depletion or cytoskeleton disruptions (Zhou and Hancock, 2015), highlighting the importance of polybasic sequences in proper signal propagation (Johnson et al., 2012). In addition, positively charged membrane-anchored proteins have been shown to induce PIP2 nanoclustering by charge stabilization (Gc et al., 2016), and equivalent effects for PIP3 have been proposed (Salamon and Backer, 2013). PIP3 and PIP2 are important signaling molecules (Krause and Gautreau, 2014). Similarly, the membrane-interacting domain of Rac1 is built up of an unspecific geranylgeranyl isoprenoid lipid and a repetition of basic residues that confer specificity for the negatively charged lipids PIP2, PIP3 (Heo et al., 2006), and phosphatidylserine (Finkielstein et al., 2006; Picas et al., 2016; van den Bogaart et al., 2011). Yet despite its fundamental role, it is still unknown whether the RhoGTPase Rac1 forms nanoclusters.

In this work, we used single-molecule localization microscopy in live cells (SPT-PALM) (Manley et al., 2008) to address the architecture and dynamics of Rac1 in the basal plasma membrane of NIH 3T3 cells. We found that Rac1 displays static and diffusing states and that Rac1 immobilization is due mainly to its partitioning into nanoclusters. Rac1 immobilization and nanoclustering are enhanced at the front of the cell and correlate with regions of high Rac1 activity. The polybasic anchor of Rac1 is sufficient to drive nanocluster formation, but results obtained from Rac1 mutants show that interactions with GEFs, GAPs, and effectors are required to enrich nanoclusters at the front of the cell. Using optogenetics combined with single-molecule imaging, we causally established that activation of cycling wild-type Rac1 leads to its immobilization and that interactions with effectors are the most efficient in promoting Rac1 immobilization, similarly to what has been observed with H-Ras (Blaževič

et al., 2016). Two-color super-resolution images confirmed that nanoclusters at the active front of the cell are composed of at least Rac1, PIP3, and the WAVE nucleation-promoting factor. Additionally, by quantitatively comparing the profiles of Rac1 activity and immobilization in micro-patterned cells, we found that the fraction of Rac1 immobilization is a non-linear function of its activity, supporting the existence of an amplification mechanism by which active Rac1 is further immobilized in regions of high Rac1 activity. We propose that interactions with downstream effectors such as WAVE are responsible for this amplification by stabilizing nanoclusters and thus enhancing their lifetime.

Altogether, the heterogeneous composition of Rac1 nanoclusters suggest that they operate as signaling platforms where GEFs, GAPs, and effectors are concentrated and where the size of nanoclusters is tightly regulated by cycling between active and inactive states. Importantly, our results show that nanoclusters can be distributed as subcellular gradients. Their distribution matches the activity measured by a fluorescence resonance energy transfer (FRET) biosensor, suggesting that a supramolecular level of organization mediates Rac1 signal transduction.

RESULTS

Rac1 Forms Nanoclusters

Single-molecule tracking experiments have been used in the past to study the diffusivity of Rac1 in spreading MCF7 cells (Das et al., 2015), dendritic spines (Chazeau et al., 2014), and within focal adhesion points of HeLa cells (Shibata et al., 2013). In the present work, we used a single-particle tracking photoactivated localization microscopy (SPT-PALM) (Manley et al., 2008) approach in a total internal reflection fluorescence (TIRF) microscopy configuration. TIRF microscopy allowed us to capture only molecules present in the basal membrane without the noisy contribution of cytoplasmic proteins. The benefit of SPT-PALM approaches is to yield individual localizations in live cells that can be used both to access the supramolecular organization of molecules in the membrane and to build individual trajectories revealing the mobility of the tagged proteins, as depicted in Figure 1A. Here, we used live cells stably expressing Rac1 labeled with the photoconvertible protein mEOS2, which we sparsely photoactivated to image single molecules (Figure 1B; Movie S1). Localizations and trajectories were used to build quantitative reporters of the architecture and dynamics of Rac1 at the basal plasma membrane (Figure 1C).

A density-based representation of PALM live cell images of wild-type Rac1 tagged with mEOS2 (mEOS2-Rac1-WT) revealed that Rac1 forms nanoclusters (Figure 1D), similarly to Ras proteins (Plowman et al., 2005; Zhou and Hancock, 2015). Analysis of the spatial distribution of mEOS2-Rac1-WT using a Ripley K function (L[r]-r) (Shivanandan et al., 2015) (Figure 1E) and a pair correlation photoactivated localization microscopy (PC-PALM) approach (Veatch et al., 2012) provided quantitative supports of nanocluster formation. Ripley functions (Figure 1E) exhibit a peak at 200 nm, indicating an inhomogeneous distribution of proteins on the membrane with structures of length scales on the order of hundreds of nanometers. Moreover, fitting of the pair correlation function of mEOS2-Rac1-WT (Figure S1)

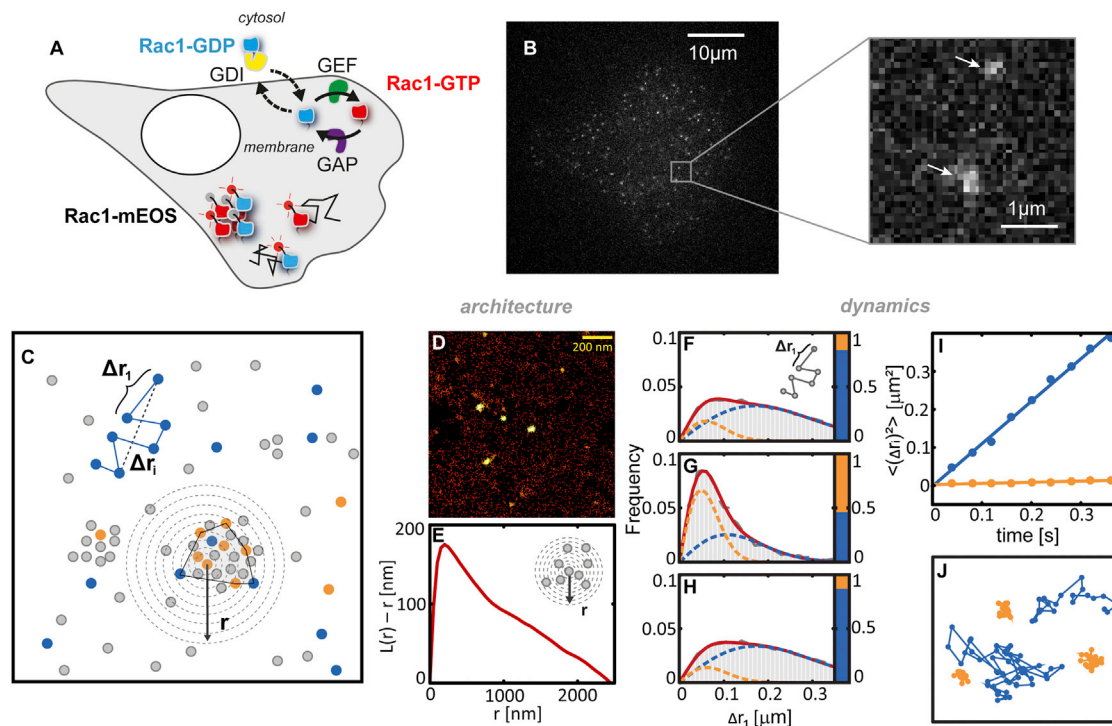


Figure 1. Rac1 Forms Nanoclusters and Presents Two Diffusive States

(A) Scheme of the mechanisms regulating Rac1 activity inside the cell. Rac1 switches between GDP (blue) and GTP (red) loaded forms and shuttles between the membrane and the cytosol. We used a TIRF SPT-PALM strategy, by fusing the photoactivatable mEOS2 fluorescent protein to Rac1. Using low power of activation, only a few mEOS2 molecules are photoconverted, giving access to localizations and trajectories of single Rac1 molecules (either GTP or GDP loaded). (B) Example of a frame from a single movie of mEOS2-Rac1-WT at the basal plasma membrane (see [Movie S1](#)) and zoom showing two individual molecules (arrows).

(C) Scheme of the parameters extracted from the single-molecule movies. Blue/orange (diffusing/immobile) spots are mEOS2 molecules that are imaged and localized from the movies. Gray spots represents mEOS2 molecule that are not imaged. From the trajectories, we extracted Δr_i , the displacement for a time lag t_i . From the localizations, we calculated the local density as a function of r , the distance from the center of a molecule (Ripley function). We identified nanoclusters using a DBSCAN algorithm. Nanoclusters were segmented using the convex hull (polygon).

(D and E) A PALM image (D) (color bar, 0–60 neighbors) of Rac1 reveals its nanocluster organization that yields a peak in the Ripley function (E).

(F–H) Single-translocation histograms (gray), Δr_i , between consecutive frames in the whole cell (F), inside nanoclusters (G), and outside nanoclusters (H) cannot be fitted with a single Brownian population. When fitted with two states, they yield a quasi-static component (orange) and a freely moving one (blue) with different population sizes. The sum of the two components is given by the red curve. Inside nanoclusters, the amount of immobilization (represented by the bar graph on the right side of plots) is much higher than outside.

(I) The mean square displacement recovered from histogram fits is linear with increasing time interval ([Figure S4](#)), and their slopes yield diffusion coefficients of $D_{\text{mobile}} = 0.28 \mu\text{m}^2/\text{s}$ for the mobile state and $D_{\text{static}} = 0.008 \mu\text{m}^2/\text{s}$ for the static state. The origin of the mobile state line yields a localization precision of $31 \pm 3 \text{ nm}$.

(J) Representative trajectories of the two populations.

Details on methods can be found in [Experimental Procedures](#).

required two components: a Gaussian one corresponding to the localization accuracy associated with multiple observations of the same molecule and an exponential one decaying over a length scale of 100–200 nm, which accounts for the existence of nanoclusters. In contrast, the pair correlation function ([Figure S1](#)) of a transmembrane domain control ([Specht et al., 2011](#)) tagged with mEOS2 can be properly fitted with only the Gaussian component. To further exclude the eventuality of spurious nanocluster identification due to the consecutive imaging of the same immobile protein, we corrected PALM images of mEOS2-Rac1-WT on fixed cells by eliminating the localizations that were within the localization precision in consecutive frames. The corrected images yielded virtually identical images than the uncorrected ones ([Figure S1](#)).

We next checked if Rac1 nanoclusters are also present for endogenous Rac1. We acquired “stochastic optical reconstruction microscopy” (STORM) images in fixed cells of immunolabeled endogenous Rac1. Resulting images also show nanoclusters ([Figure S1](#)) and show pair correlation functions that cannot be fitted solely with a Gaussian component ([Figure S1](#)). Altogether, our measurements provide strong evidence that Rac1 forms nanoclusters at the plasma membrane.

Rac1 Is Immobilized in Nanoclusters

As previously shown for Ras, nanoclusters can arrest proteins and thus modulate lateral diffusivity on the membrane. We thus assessed if nanoclusters also immobilized Rac1 molecules. We extracted trajectories of single molecules of mEOS2-Rac1-WT

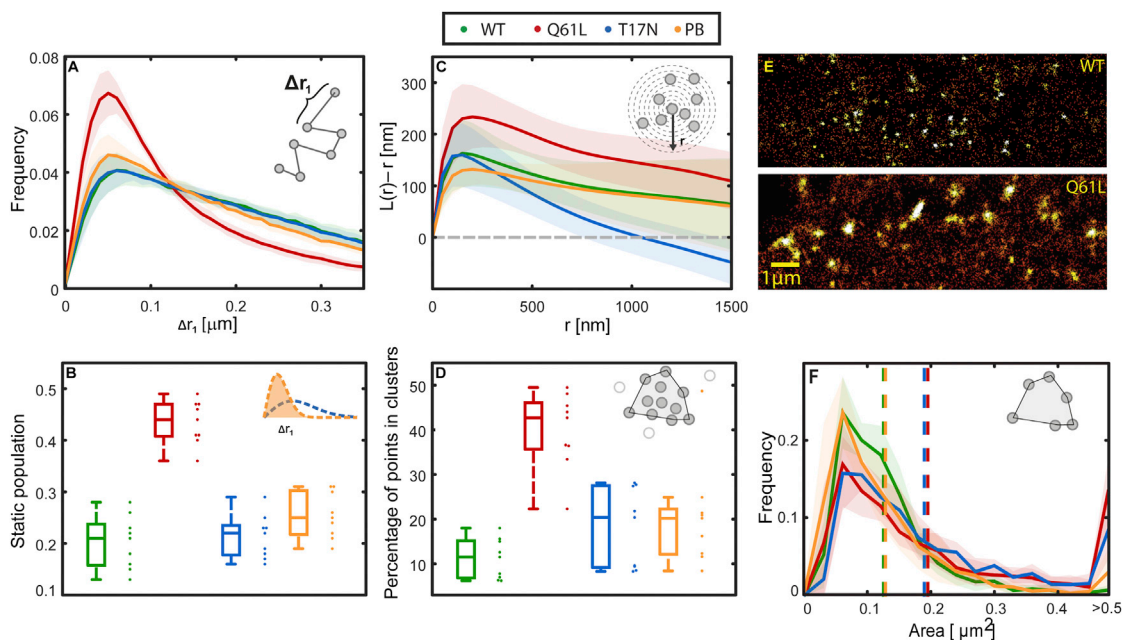


Figure 2. Active Rac1 Presents Decreased Diffusivity and Increased Nanoclustering

(A) Single-translocation histograms obtained from single-molecule movies of wild-type (mEOS2-Rac1-WT, green), active (mEOS2-Rac1^{Q61L}, red), and inactive (mEOS2-Rac1^{T17N}, blue) Rac1 mutants and the polybasic-CAAX control membrane anchor (PB-CAAX, orange). The histograms are fitted with two independent populations of different diffusivity (see [Experimental Procedures](#)).

(B) The integrated relative area of the static population obtained in (A) is larger for mEOS2-Rac1^{Q61L} than for mEOS2-Rac1-WT, mEOS2-Rac1^{T17N}, and the polybasic-CAAX membrane anchor, showing that the degree of immobilization increases with Rac1 activity.

(C) The peak in the Ripley function $L(r)-r$, measuring the degree of Rac1 nanoclustering, is higher for mEOS2-Rac1^{Q61L}, showing that increasing activity of Rac1 produces, as well, higher nanoclustering.

(D) The ratio of points contained within nanoclusters obtained with a DBSCAN algorithm is more than twice as large for mEOS2-Rac1^{Q61L}.

(E) PALM images (color bar, 0–60 neighbors) of representative nanoclusters of mEOS2-Rac1-WT (top) and mEOS2-Rac1^{Q61L} (bottom) exhibit a significant difference in nanocluster sizes.

(F) Mean nanocluster surface areas shown in dashed lines are larger for mEOS2-Rac1^{Q61L} and mEOS2-Rac1^{T17N}. Note that the last point of all curves increases as it contains all residual values greater than $0.5 \mu\text{m}^2$.

(A) and (F) are means of nine different single-cell histograms, and error bars are calculated as SDs. The mean Ripley function in (B) is a mean of nine different single-cell Ripley functions with error bars calculated as SDs. Boxplots in (B) and (D) represent the medians of measurements on nine different cells.

(see [Experimental Procedures](#)) and built histograms of the displacements of molecules between consecutive frames (Figures 1F–1H), called single translocations hereafter. Such histograms could not be fitted with a model of a single Brownian species and required two populations (Schütz et al., 1997). The analysis of the distribution of single displacements for increasing time intervals clearly supported the bimodality of the diffusion (Figures 1I and S2). The diffusivity of the slower state ($D_{\text{slow}} = 0.008 \pm 0.003 \mu\text{m}^2/\text{s}$) is within the localization precision of our experimental system and can be considered as static. In the rapid state, the diffusion coefficient is $D_{\text{fast}} = 0.28 \pm 0.003 \mu\text{m}^2/\text{s}$, in agreement with the lateral diffusion coefficient of a freely moving membrane-bound protein. Trajectories shown in Figure 1J are representative of each state of Rac1 mobility.

We looked for a preferential partitioning of the static state in nanoclusters. Nanoclusters were identified and segmented using a density-based scanning algorithm (Tran et al., 2013) such that trajectories could be sorted as belonging or not to nanoclusters (see [Experimental Procedures](#)). Histograms of single translocations in Figure 1G show that trajectories within nanoclusters present a 5-fold higher static population than those in regions

outside nanoclusters (Figure 1H). We estimated that 15% of all mEOS2-Rac1-WT immobilizations happen inside nanoclusters (Figure S2). Although this number might be largely underestimated because nanoclusters of smaller sizes are missed by our method, this result shows that partitioning into nanoclusters is one mechanism by which Rac1 becomes immobilized.

Active Rac1 Presents an Increased Fraction of Immobilization and Nanoclustering

We next assessed the relationship between activation and immobilization of Rac1 by examining the diffusivity and nanocluster partitioning of different Rac1 mutants. Figure 2A shows single-translocation histograms of mEOS2-tagged wild-type Rac1 (mEOS2-Rac1-WT), constitutively active Rac1 (mEOS2-Rac1^{Q61L}), dominant-negative Rac1 (mEOS2-Rac1^{T17N}), and the CAAX-polybasic region that works as a membrane anchor after post-translational modifications. Figure 2B shows the distribution of the static populations sizes obtained from fitting the translocation histograms (Schütz et al., 1997). Interestingly, the polybasic membrane anchor presents a similar degree of immobilization and nanoclustering as the mEOS2-Rac1-WT,

suggesting that nanocluster formation is inherent to the Rac1 CAAX-polybasic C-terminal domain of the protein. This phenomenon is consistent with previous reports on the capacity of the C-terminal polybasic domain to mediate Rac1 oligomerization (Zhang et al., 2001). However, mEOS2-Rac1^{Q61L}, which has the largest static population (Figure 2B), the highest peak in Ripley K functions (Figure 2C), and the highest percentage of localizations within clusters (Figure 2D), shows that immobilization and nanoclustering have a positive correlation with Rac1 activity. These results, together with previous reports (Shibata et al., 2013; Das et al., 2015; Chazeau et al., 2014), provide robust evidence that in migrating fibroblasts GTP-loaded active Rac1 is less mobile than its inactive counterpart.

In addition to the differences in nanocluster partitioning among Rac1 mutants, PALM images (Figure 2E) of representative nanoclusters for mEOS2-Rac1-WT and mEOS2-Rac1^{Q61L} show a clear difference in size. mEOS2-Rac1-WT displays nanocluster sizes comparable with those of the polybasic-CAAX membrane anchor, whereas mEOS2-Rac1^{T17N} and mEOS2-Rac1^{Q61L} display twice larger nanoclusters (Figure 2F). The quantification of the number of proteins per nanoclusters is a difficult task because of the blinking of mEOS2 (Durisic et al., 2014; Fricke et al., 2015). However, on average, we estimated that mEOS2-Rac1^{Q61L} and mEOS2-Rac1^{T17N} mutants present 233 ± 110 and 232 ± 49 localizations per nanoclusters, whereas mEOS2-Rac1-WT and the polybasic-CAAX anchor present 97 ± 33 and 83 ± 38 localizations. The localizations can be used as a loose estimate of the real number of molecules per nanocluster. If we consider that in our experimental conditions, a single molecule is counted on average 2.3 times and that the photophysics of mEOS2 allow sampling of only 78% of the molecules (Durisic et al., 2014), the number of molecules per nanocluster can be estimated as 0.55 times the number of localizations per nanocluster. Hence mEOS2-Rac1-WT nanoclusters are composed of approximately 50 molecules, about five times more than the number of Ras molecules in its nanoclusters (Hancock and Parton, 2005). Larger areas and larger numbers of localizations per nanoclusters present in mEOS2-Rac1^{Q61L} and mEOS2-Rac1^{T17N} mutants show that the cycling between active and inactive states is a major factor regulating nanocluster size.

Cycling rates are of high relevance in signaling. Fast cycling of Rac1, but not locking of Rac1 in its GTP-bound form, was shown to transform cells, like the oncogenic activation of upstream GEFs (Wertheimer et al., 2012; Davis et al., 2013). These results suggest that the cycling kinetics of Rac1 activation determine the transduction efficiency of Rac1 downstream signaling. Given that mEOS2-Rac1^{Q61L} is locked in its GTP-bound state, we examined whether the link between diffusivity and activity identified in mEOS2-Rac1^{Q61L} was also present in cycling Rac1. To this end, we coupled single-molecule tracking experiments with optogenetic activation (Kennedy et al., 2010) (Figure 3A). In transiently transfected cos7 cells, we illuminated for 10 min a specific region of the cell to recruit at the plasma membrane the catalytic domain of the Rac1 GEF Tiam1 (Cry2-Tiam1-iRFP), thereby inducing localized activation of Rac1. Our optogenetic activations led to a 1.2- to 2.2-fold increase of Cry2-Tiam1-iRFP inside the region of activation (Figure S3). When analyzing single-translocation histograms, we found that only mEOS2-

Rac1-WT displayed an increase in the static population size upon recruitment of Cry2-Tiam1-iRFP (Figure 3B). We acquired single-molecule movies of all mEOS2-tagged Rac1 mutants and the polybasic-CAAX anchor before and after recruitment (Figures 3C–3H), and we mapped the diffusivities over cells using a recently developed methodology (see Experimental Procedures). The polybasic-CAAX membrane anchor and mEOS2-Rac1^{T17N} cannot engage effectors, and mEOS2-Rac1^{Q61L} is already in the active state and cannot increase its interaction with effectors. Taking into account that Cry2-Tiam1-iRFP has a diffusivity of $0.1 \pm 0.03 \mu\text{m}^2/\text{s}$ (Valon et al., 2015), comparable with that of the mobile population of Rac1, we attributed the increased immobilization of mEOS2-Rac1-WT to an increase in the amount of active molecules and the consequent interaction with effectors. These optogenetic experiments show that for cycling Rac1, there is a causal relationship between activation and immobilization.

Rac1 Presents Similar Gradients of Immobilization, Nanocluster Density, and Activity

Motivated by previous studies that identified spatial profiles of RhoGTPases activity across cells (Yang et al., 2016), we aimed to compare them with immobilization profiles and nanocluster distribution. To this end, we plated cells on crossbow fibronectin micropatterns to obtain a normalized cell shape and organization (Théry et al., 2006). The “front” of these cells exhibits ruffling (Viaud et al., 2014) and mimics a lamellipodium rich in branched actin. This approach allows the comparison of several measurements taken in different experiments and offers a template for a multiplex mapping approach (Figure 4A). Because of the reduced cell-to-cell variability, we were able to average and map in the same referential the fraction of immobile molecules, the nanocluster densities, and the FRET ratiometric images (Figures 4B–4F).

We first acquired single-molecule movies (2,000–5,000 frames at 25 Hz) with densities comparable to Figure 1B ($0.2 \text{ molecules}/\mu\text{m}^2$). We then mapped Rac1 diffusivity in 9–18 individual cells for each mutant, and we averaged those maps (Figure 4B) after morphing each cell onto the average shape (see Experimental Procedures). mEOS2-Rac1-WT, mEOS2-Rac1^{Q61L}, and mEOS2-Rac1^{T17N} exhibit diffusivity gradients from the front to the middle of the cell with a region of lowest diffusivity along the cell front-most region. mEOS2-Rac1^{Q61L} presents the greatest contrast in diffusivity between front and middle. Because a given local average diffusion coefficient corresponds to a given local proportion of immobile molecules, diffusivity maps can be interpreted in terms of local fraction of immobilization (see color bar in Figures 4B and 4D). By taking into account the diffusion constant of the slow and fast states derived from tracking experiments, average diffusivities $D_{\text{mean}} = f_i \cdot D_{\text{slow}} + (1 - f_i) \cdot D_{\text{fast}}$ yielded immobilization fractions f_i . In the same single-molecule movies, nanoclusters were identified, and their spatial densities mapped onto the cell (see Experimental Procedures). As expected given our previous results, the nanocluster density map in Figure 4C shows that mEOS2-Rac1-WT, mEOS2-Rac1^{Q61L}, and mEOS2-Rac1^{T17N} present nanocluster enrichment at the front of the cell, supporting again the link between nanocluster partitioning and immobilization.

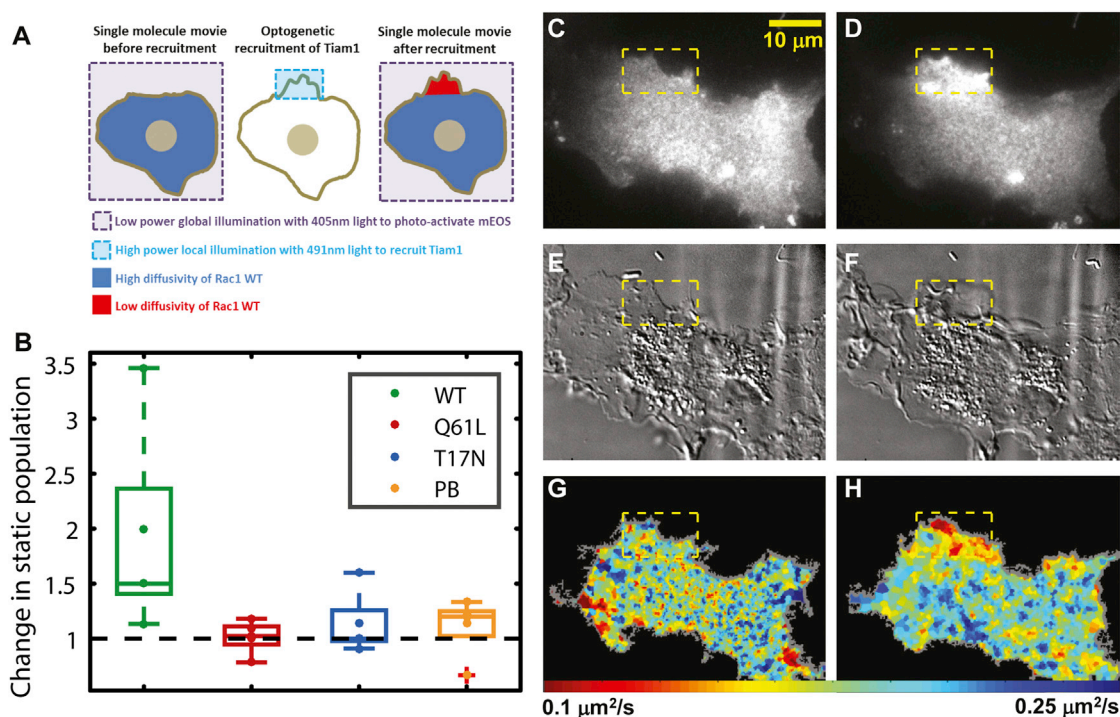


Figure 3. Diffusivities as a Function of Rac1 Activity Modulated through Optogenetics

(A) Schematic of the experiment. (Left) A single-molecule movie is acquired by photoconverting mEOS2-Rac1 with low global 405 nm illumination to avoid significant optogenetic recruitment. (Middle) A 10 min local recruitment step is performed, and higher power 491 nm light is used to illuminate a region of interest and recruit Tiam1, a GEF of Rac1, with local specificity. (Right) Another single-molecule movie is acquired.

(B) Initial and final single-molecule movies were localized and tracked to yield single-translocation histograms as shown in Figure 1. The ratio of the static population within the activation region between the final and initial movie shows an increase of the immobilization upon optogenetic activation only for mEOS2-Rac1-WT.

(C–F) iRFP channel images before (C) and after (D) optogenetic activation show Tiam1 recruitment efficiency, and DIC images before (E) and after (F) optogenetic activation expose ruffling induced by Tiam1 recruitment.

(G and H) Diffusivity maps before (G) and after (H) optogenetic activation exhibit immobilization of mEOS2-Rac1-WT confined to the activation region. Seven cells were used for each condition.

We also measured the Rac1 activity map on crossbow micro-patterns with a FRET biosensor (Moshfegh et al., 2014). Assuming that the distribution of the inactive Rac1 is uniform, as suggested by the large pool of inactive Rac1, the pixel intensities in ratiometric FRET images are proportional to the local amount of active Rac1. Under this assumption, the FRET signal provides a linear measure of the relative Rac1 activity. The nanocluster distribution and diffusion map of the WT (Figures 4D and 4E) match the biosensor signal (Figure 4F), all showing a decaying gradient from the front to the center. Thus, in an unperturbed condition, we see a clear positive correlation between Rac1 activity, immobilization, and nanocluster density.

GEF/GAP Cycling Rather Than GDI-Mediated Membrane Shuttling Regulates Rac1 Activation Patterns in Spread Cells

Localized shuttling of Rac1 to the membrane is one of the processes potentially regulating Rac1 activation. The relative weight of local activation versus local delivery in cell polarity establishment has been addressed before for *cdc42* (Woods et al., 2015; Hodgson et al., 2016). Localized delivery has been pro-

posed as a critical mechanism in the establishment of cell polarity in cells minutes after attachment (Das et al., 2015). Yet the importance of localized delivery may differ in the context of already spread cells. It has been shown that the attachment and spreading processes involve a particular set of signaling pathways (Schwartz, 1997), which may not be triggered once cells have reached a steady state. To evaluate the role of localized delivery in the context of already spread cells, we performed a plasma membrane turnover analysis on the basis of photobleaching experiments.

Fluorescence recovery after photobleaching (FRAP) experiments of the green form of mEOS2-Rac1-WT on the whole basal membrane with TIRF microscopy showed that the shuttling of Rac1 to the membrane slows down along the spreading process. By performing FRAP experiments 30 min and 3 hr after plating, we found that fluorescence recovery times increased from about 6 to about 20 min (Figure S4). A turnover time of 20 min in fully spread cells is of the same order of magnitude as the plasma membrane recycling. This experiment shows that GDI-mediated shuttling occurs on a longer timescale than protrusion/retraction cycles. Therefore, we considered that the

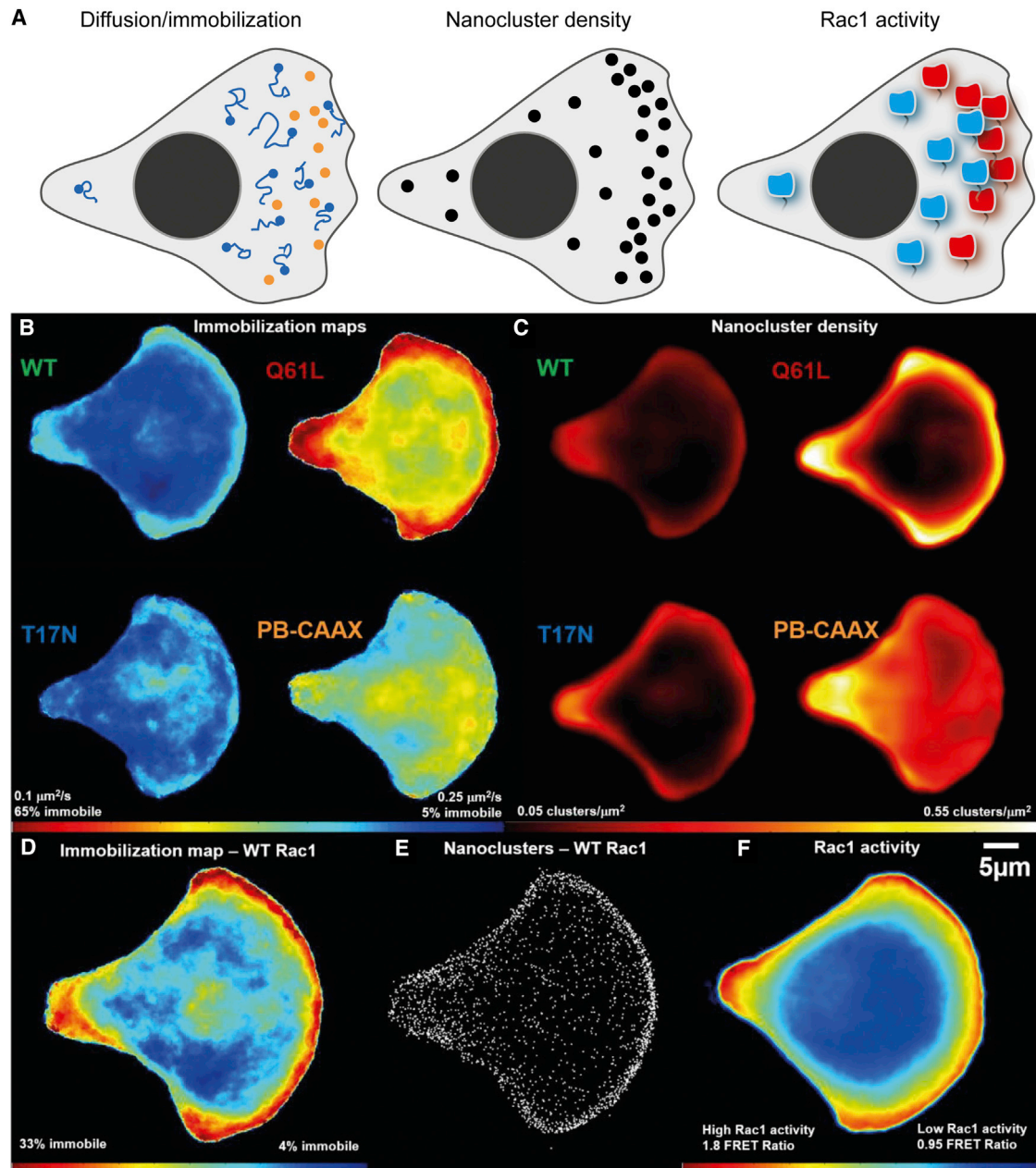


Figure 4. Rac1 Diffusivity, Activity, and Nanocluster Distribution along Normalized Polarized Cell States Imposed by Fibronectin Crossbow Micro-Patterns

(A) Cartoon describing the three parameters presented in this figure.

(B) Immobilization/diffusion maps were obtained from 9 cells per mutant and 18 cells for the mEOS2-Rac1-WT. Cells were tessellated with a Voronoi mesh, the local diffusion coefficient in each region was estimated from the single-molecule localizations using an inference approach (see [Experimental Procedures](#)), and cells were wrapped onto the average cell shape and averaged (see [Experimental Procedures](#)). Immobilization maps of Rac1 mutants show decreased overall diffusivity for mEOS2-Rac1^{Q61L} and an inhomogeneous diffusivity distribution for all three forms of Rac1, with lower diffusivity at the front and back, in contrast to the polybasic anchor, which exhibits uniform diffusivities.

(C) Nanocluster density maps (see [Experimental Procedures](#)) show a higher nanocluster density for mEOS2-Rac1^{Q61L} and an increased nanocluster density at the front of the cell for all three Rac1 mutants.

(D–F) Comparison of immobilization maps with a maximized dynamic range (D), nanocluster distribution of wild-type Rac1 (E), and Rac1 activity maps obtained from FRET biosensor ratios (F); all exhibit a gradient from front to center.

predominant mechanism for the generation and maintenance of activation profiles in our experimental conditions was the localized cycling of Rac1, not its localized delivery.

Rac1 Polybasic Tail Is Sufficient for Nanocluster Partitioning, but Interactions with Rac1 Partners Are Required for Nanocluster Enrichment in Active Regions of the Cell

To further dissect the role of Rac1 molecular interactions in regulating nanocluster distribution, we next quantified the enrichment of nanoclusters in the front of the cell for all mutants, exploiting the fact that they have distinct interacting partners. Among the Rac1 interactome, the best-characterized Rac1 partners are GEFs, GAPs, and the direct effectors. mEOS2-Rac1-WT can interact with all of them. mEOS2-Rac1^{Q61L} can interact with GAPs and effectors and perhaps also with GEFs, as demonstrated for Ras proteins (Hobbs et al., 2016). However, mEOS2-Rac1^{T17N} exhibits high affinity for GEFs but cannot bind effectors or GAPs.

To quantify the tendency of Rac1 to cluster in different parts of the cell, we divided the crossbow into three different regions, as shown in Figure 5A, and measured the density of nanoclusters (Figure 5B) and the percentage of Rac1 detections in nanoclusters for each region (Figure 5C). We chose to exclude the back of the cell from the analysis given that its morphology departs from the canonical lamellipodia. Cells plated in crossbow micropatterns present a “small front” at the back, characterized by a high concentration of cortactin (Théry et al., 2006) and high branching. In this aspect, they differ from freely migrating cells that exhibit a retracting tail.

A similar number of immobilizations as the one reported here has been seen for the polybasic-CAAX motif inside and outside of focal adhesions in HeLa (Shibata et al., 2013) and MEF (Rossier et al., 2012) cells and in dendritic spines (Chazeau et al., 2014). However, during spreading of MCF7 cells, the polybasic-CAAX anchor does not seem to present a slowly diffusing population (Das et al., 2015). Here, we identified that 18% of the polybasic-CAAX anchor of Rac1, similarly to that of H-Ras (Pezzarossa et al., 2015), is organized into nanoclusters (Figure 5C) and that 23% of the immobile population can be found within nanoclusters (Figure S4).

Yet the interactions responsible for polybasic-CAAX nanocluster formation are insufficient to enrich Rac1 nanoclusters at the front of the cell (Figure 5D). In contrast, mEOS2-Rac1-WT, mEOS2-Rac1^{T17N}, and mEOS2-Rac1^{Q61L} (Hobbs et al., 2016; Um et al., 2014) exhibit a 2-fold increase in nanocluster density at the front (Figure 5D), very likely due to additional interactions. These results suggest that GEFs, GAPs, and effectors are sufficient for a relative enrichment of Rac1 nanoclusters at the front of the cell. The significant increase of nanoclustering in mEOS2-Rac1^{Q61L} suggest additionally that interactions with effectors, strongly present in this mutant, are the most effective in promoting nanocluster partitioning.

To test this hypothesis, we looked for the presence within nanoclusters of WAVE2, a major Rac1 effector, and PIP3, which recruits GEFs and GAPs. We acquired two-color PALM/STORM images of cells expressing mEOS2-Rac1^{Q61L} and immunolabeled WAVE2 or PIP3. Supporting our hypothesis, we observed

a colocalization of mEOS2-Rac1^{Q61L} and WAVE2 (Figures 5E–5G) and a colocalization between mEOS2-Rac1^{Q61L} and PIP3 (Figures 5G and 5H) in some of the nanoclusters at the front.

Rac1 Nanoclusters Do Not Depend on the Actin Cytoskeleton

Actin has been proposed as an inducer of membrane protein nanoclusters either via the formation of transient contractile regions at the plasma membrane that stabilize liquid order domains and couple to extracellular glycosylphosphatidylinositol-anchored proteins (GPI-Aps) or through the direct interaction of transmembrane proteins with actin filaments (Raghupathy et al., 2015; Plowman et al., 2005). Indeed, nanoclusters of different Ras isoforms exhibit selective dependence on actin. Figure 5I shows that treatment with latrunculin and cocktails that freeze actin dynamics (Peng et al., 2011) does not have an effect on the diffusivity of any of the Rac1 mutants or the polybasic-CAAX anchor control. These results suggest that, like H-RasGTP (Plowman et al., 2005; Huang et al., 2013; Köster et al., 2016), Rac1 is found in nanoclusters that do not depend on the actin cytoskeleton.

Partitioning of Rac1 in Nanoclusters Is Amplified in Regions of High Rac1 Activity

To further assess the role of interactions in nanoclustering, we performed a detailed quantification of Rac1 immobilization fractions, nanocluster density, and Rac1 activity at the cell front (Figure 5J). Immobilization fraction and nanocluster density profiles can be perfectly overlaid, whereas activity gradient shows a twice-larger spatial extent (Figure 5J). Plotting the nanocluster density as a function of the activity shows a non-linear relationship between the two (Figure 5K). Immobilization fractions are constant for low Rac1 activity. However, for increasing Rac1 activity, the immobilization fraction increases drastically. This observation points to the existence of an amplification mechanism by which active Rac1 molecules have an enhanced propensity to partition into nanoclusters in regions of high Rac1 activity. Note that this amplification holds under the assumption of a linear relationship between the FRET ratio and the relative Rac1 activity (see above).

DISCUSSION

We performed a single-molecule analysis of Rac1 mobility and supramolecular architecture in migrating fibroblasts. Our main finding is that a significant fraction of Rac1 at the plasma membrane is found in nanoclusters of a few tens of molecules, which are distributed as gradients matching Rac1 subcellular patterns of activity.

Because the polybasic anchor of Rac1 forms nanoclusters and because nanocluster partitioning is independent of actin, Rac1 nanocluster formation is probably driven by electrostatic interactions of its polybasic-CAAX anchor with negatively charged lipids such as PIP2 and PIP3, as previously proposed (Li et al., 2014). Nanoclusters would form and dissociate spontaneously, without the requirement for active processes or biochemical modifications. Previous studies on the formation of nanoclusters of different Ras isoforms (Zhou and Hancock,

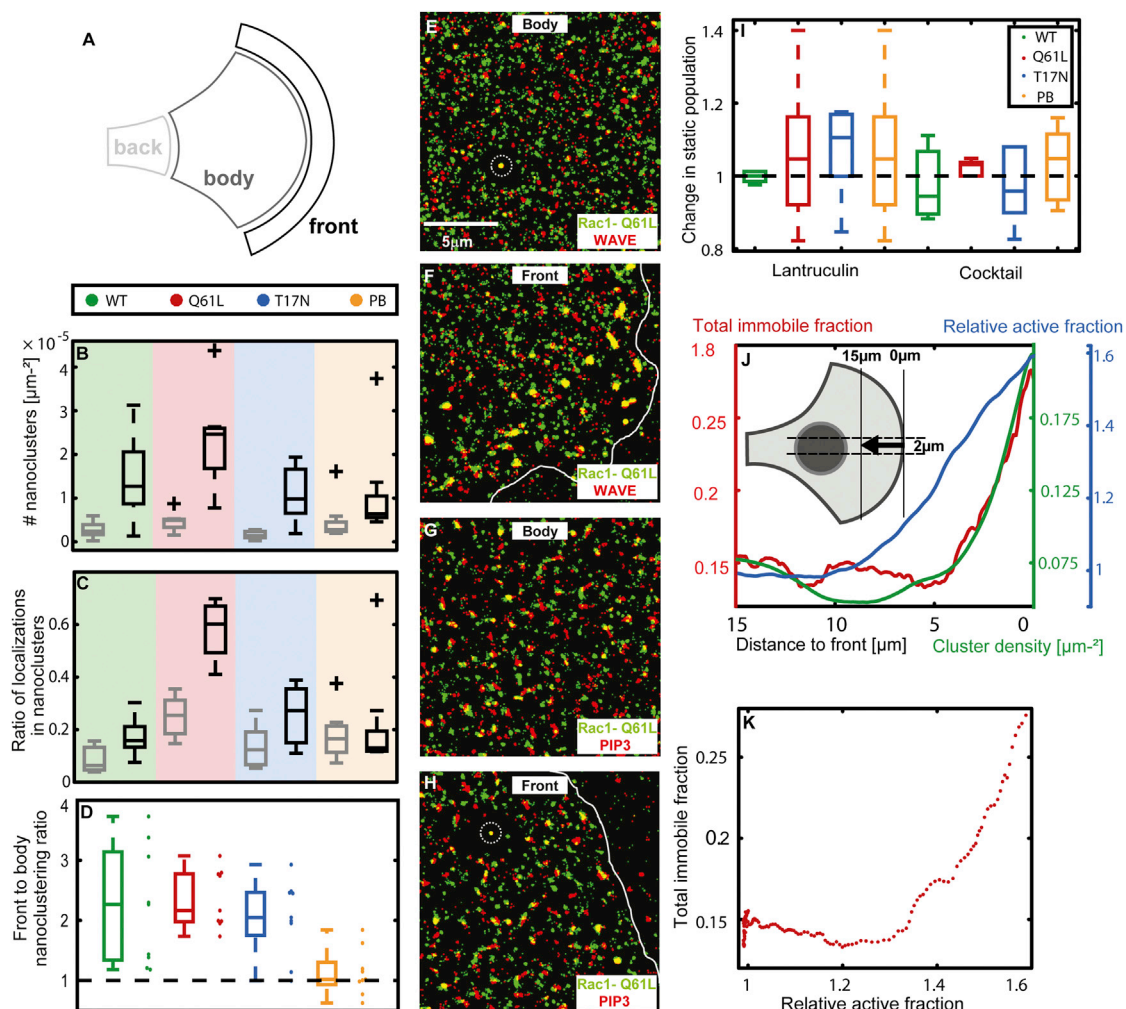


Figure 5. Rac1 Nanoclusters, Activity, Immobilization, and Composition Distribution

(A) Cells were divided into regions called front, body, and back, as depicted in the sketch.

(B and C) The number of nanoclusters per surface area (B) and the fraction of points in nanocluster (C) were measured for each region in each cell and then averaged across nine cells. Both the number of nanoclusters and the total amount of points in nanoclusters are increased at the front of Rac1 mutants in comparison with the body but are comparable for the polybasic-CAAX anchor.

(D) The front-to-body ratio of points in nanoclusters is about 2 for all Rac1 mutants and about 1 for the polybasic-CAAX anchor.

(E–H) STORM-PALM images of fixed cells plated in crossbow micropatterns expressing mEOS-Rac1^{Q61L} (green) were constructed using primary antibodies against the WAVE complex (E and F) and PIP3 (G and H), and secondary antibodies (red) tagged with Alexa Fluor 647 for front and body regions. The colocalization of mEOS-Rac1^{Q61L} and Alexa Fluor 647 is shown in yellow. mEOS-Rac1^{Q61L} and WAVE exhibit nanoclusters of high colocalization at the front of the cell but negligible colocalization in the body. mEOS-Rac1^{Q61L} also colocalizes with PIP3, but the contrast between front and body is less striking than for WAVE.

(I) In order to compare immobilization, nanoclustering, and activity profiles, we averaged 2 μm horizontal stripes across the cell center (inset) of all maps shown in Figure 4. The invariance of the static population fraction for all mutants upon treatment with either lantrunculin or a drug cocktail that freezes actin dynamics (Peng et al., 2011) suggest that the formation of Rac1 nanoclusters does not depend on actin.

(J) On the first 15 μm behind the cell edge, the profile of the Rac1 relative activity (blue) has a decay length two times larger than the profiles of Rac1 immobile fraction (red) and Rac1 nanocluster density (green).

(K) Immobilization fractions show a non-linear dependence with relative active fractions.

2015; Plowman et al., 2005) highlighted the importance of the protein anchor in signaling. These studies identified the role of cholesterol, different membrane anionic lipids, nucleotide load, degree of palmitoylation, and protein conformations in the formation and composition of Ras nanoclusters. The anchor of Rac1 resembles K-Ras in the presence of a polybasic region but rather resembles H-Ras in its mono-palmitoylation. Palmi-

toylation has been shown to induce partitioning of Rac1 into cholesterol-rich liquid-ordered regions (Navarro-Lérida et al., 2012) of sizes in the range of tenths of micrometers. One way to reconcile these data with ours is to consider that nanoclusters belong to larger structures, micrometer sized, which depend on actin and cholesterol but do not play a role in Rac1 immobilization.

Supporting the role of charged lipids in Rac1 nanoclustering, a fraction of PIP2 and PIP3 form nanoclusters in PC12 (van den Bogaart et al., 2011; Wang and Richards, 2012) and INS-1 (Ji et al., 2015) cells. These lipid nanoclusters might be segregated (Ji et al., 2015), and their diameters are 70 nm for PIP2 and 120 nm for PIP3. The spatial distribution of PIP3 and PIP2 nanoclusters was not addressed here, but other studies reported nonoverlapping distributions of PIP3 and PIP2 at the cellular scale (Petrie et al., 2009). PIP3 accumulates at the leading edge and adhesions zones during guided cell migration of fibroblasts (Haugh et al., 2000) and in membrane protrusions during random cell migration (Weiger et al., 2009). In addition, PIP3 directly recruits WAVE to the membrane of polarized cells through a basic sequence in its N-terminal part in an actin-independent manner (Oikawa et al., 2004; Lebensohn and Kirschner, 2009). Our results suggest an additional regulatory function of PIP2 and PIP3, that of inducing nanoclustering of Rac1 via the interaction with its polybasic membrane anchor through coulombic interactions (Li et al., 2014; van den Bogaart et al., 2011; Honigsmann et al., 2013).

We found that Rac1 nanoclusters are enriched at the front of the cell, contrarily to the nanoclusters of the polybasic anchor. The subcellular enrichment of nanoclusters is mediated by a second set of interactions, with the GEFs, GAPs, effectors, and possibly other Rac1 partners. In our experiments, the anisotropic spatial cue is given by the asymmetric adhesive crossbow patterns. This constraint yields an organized cell architecture with focal adhesions enriched at the adhesive borders (Théry et al., 2006) that is expected to give rise to an anisotropic distribution of GEFs and GAPs in two different ways. First, direct recruitment and activation of Rac1 to early focal adhesions, the so-called focal complexes at the lamellipodial edge, has been shown to happen via the GEFs β -Pix, DOCK180, Trio, Vav2, Tiam1, and α -Pix (Lawson and Burridge, 2014) in a cell type-dependent manner. In particular, Tiam1 accumulates at focal complexes of migrating cells, and its activation mechanisms have been elucidated (Wang et al., 2012). But also, indirect recruitment and activation of Rac1 in the proximity of focal complexes can happen via PIP3. Indeed, some Rac1 GEFs are recruited with high efficiency by PIP3, but not by other anionic lipids, because of the specificity of pleckstrin homology (PH) domains (Stahelin et al., 2014). The imposed asymmetry in fibronectin yields an intracellular anisotropy of focal adhesions and a consequent anisotropy of all the signaling components from PIP2 to PIP3, GEFs, and GAPs that results in an enrichment of cortactin at the front of crossbow micropatterns (Théry et al., 2006).

Among Rac1-interacting partners, effectors appeared to be the most effective in biasing nanocluster distribution. Indeed, mEOS2-Rac1^{O61L} presents considerably higher nanoclustering and colocalizes strongly with WAVE in super-resolution images. The importance of WAVE in promoting Rac1 nanoclustering can explain the amplification we observed in Figure 5K. Because the distribution of Rac1 effectors correlates with the local density of nanoclusters, we propose that the enrichment of nanoclusters at the front is due to an increased residence time of active Rac1 within nanoclusters rather than an enhanced seeding of nanoclusters. The amplification mechanism would then operate in the following way: active Rac1 and PIP3 (Oikawa et al., 2004;

Lebensohn and Kirschner, 2009) recruit effectors to nanoclusters that become trapped and are capable of further retaining active Rac1 within nanoclusters. As a result, this mechanism would act as Rac1 positive feedback.

In this work, we propose that nanoclusters comprising active Rac1 molecules act as signaling units regulating downstream transduction. Such nanodomains have already been observed for other membrane-bound signaling proteins, and several hypotheses have been proposed to explain their functional relevance (Cebecauer et al., 2010). High local concentrations within nanoclusters could set a threshold for signal transduction. Weak interactions can be stabilized by cooperativity in nanoclusters enabling the activation of downstream signaling cascades, as recently shown with the aPKCs kinase transducing intracellular calcium (Bonny et al., 2016). For Ras (Tian et al., 2007), it was shown that nanoclusters act as a signal-processing step converting analog inputs (concentrations of ligands) into digital ones (numbers of nanoclusters) and giving rise to other analog outputs (levels of intracellular active species) further processed downstream. The functional role of analog-to-digital-to-analog processing is not fully understood, but it has been proposed to provide high-fidelity responses (Tian et al., 2007). More recently (Roob et al., 2016), it was proposed that nanoclusters of about ten molecules exhibit optimal fidelity. Digitalization reduces the numbers of output states but also reduces the noise in the system, and a trade-off between the two maximizes information transmission.

For Rac1, we do not know yet the functional role of nanoclustering, but we can hypothesize that the same concepts hold true. Rac1 nanoclusters may work as a means to generate discrete signals by setting up WAVE thresholds that modulate actin polymerization in a non-linear way, as suggested by the need for coincident anionic lipids, phosphorylation of WAVE, and active Rac1 (Lebensohn and Kirschner, 2009). In addition, Rac1 nanoclusters may modulate reaction rates by modifying the local concentration of reactants (Groves and Kuriyan, 2010; Castellana et al., 2014), adding an additional layer of regulation aimed at refining profiles of Rac1 activity and actin polymerization. Along this line of thought, the spatial modulation of cycling rates has been observed in wound-healing experiments in oocytes (Burkel et al., 2012). Here, even if the spatial distribution of signaling molecules has already been recognized (Kholodenko et al., 2010), we show for the first time that a graded distribution of nanoclusters is a means to provide a spatially modulated digital output.

Nanoclusters can support a double role in generating high-fidelity responses. In addition to noise reduction, nanoclusters can help in the maintenance of sharp regions of signaling activity (Iyengar and Rao, 2014). Indeed, Rac1 partitioning into nanoclusters is one of the mechanisms through which Rac1 is immobilized and its diffusion spatially restricted. Previous studies (Bement et al., 2006) aimed at characterizing the link between diffusivity, cycling, and source distribution showed that decreasing the diffusion constant throughout the cell can enhance the sharpness of activity gradients. Our results show that this effect can be acting through the diffusivity gradients that follow activation profiles from the front to the back of the cell. As seen in Figure S5, immobilization gradients enable an increase in deactivation time by a factor of ~ 2 . Even though this

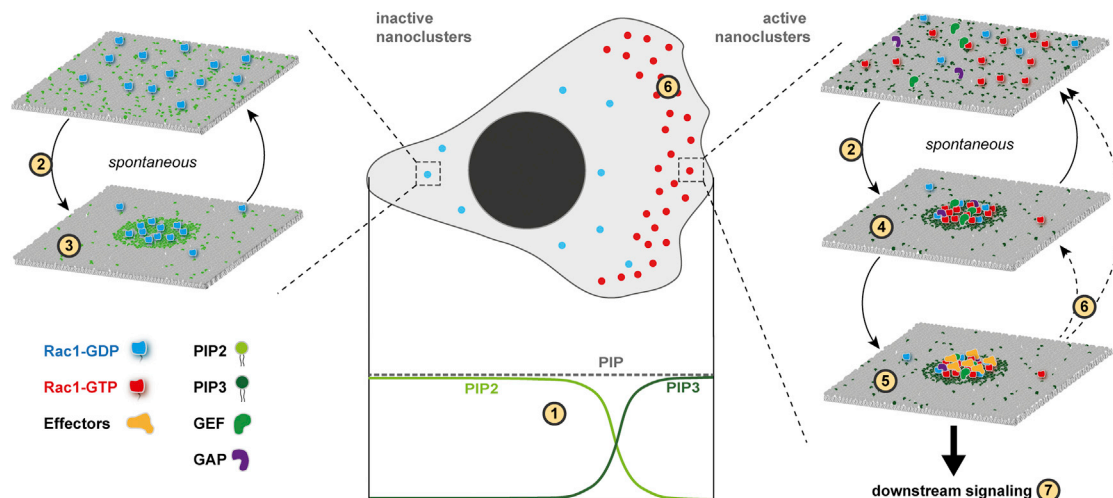


Figure 6. Model for Rac1 Nanoclustering

Opposing gradients of PIP3 and PIP2 across the cell (1) and the segregation into different clusters at the molecular level propose an enrichment of active Rac1-PIP3 nanoclusters at the front. Both active and inactive Rac1 can form nanoclusters spontaneously through electrostatic interactions (2). In the body, inactive Rac1 and PIP2 form inactive nanoclusters (3). At the front, active Rac1 and PIP3 form active nanoclusters (3), which also integrate GEFs and GAPs. These active nanoclusters recruit Rac1 effectors (5), which stabilize nanoclusters' lifetime and consequently enrich nanocluster density at the cell front (6). The heterogeneous composition of active nanoclusters suggests the existence of signaling platforms necessary for downstream signaling (7). Under this assumption, the stabilization of nanoclusters by effectors acts as positive feedback to increase the amount of Rac1 signaling where a high density of effectors is present.

might appear a mild increase, we believe that in endogenous conditions the restriction of diffusion might be a significant mechanism to maintain sharp activation gradients because the total fraction of immobile Rac1 might be higher, as suggested by the increased nanoclustering seen for endogenous Rac1 (Figure S1).

In conclusion, our findings can be summarized in the model sketched in Figure 6. Polarized migrating cells exhibit opposite gradients of PIP3/PIP2 with an enrichment of PIP3 at the front and PIP2 in the body (Petrie et al., 2009; Haugh et al., 2000; Weiger et al., 2009). Because PIP3 and PIP2 may organize in segregated nanoclusters (Wang and Richards, 2012), we believe that the front of the cell presents a larger number of PIP3 nanoclusters and the body a larger number of PIP2 ones. The affinity of the polybasic-CAAX anchor for either PIP2 or PIP3 might be comparable given that they are based on non-specific coulombic interactions, and thus nanoclusters labeled by this anchor are homogeneously distributed. However, PIP3 nanoclusters at the front recruit GEFs and GAPs and are enhancing the lifetime of Rac1 nanoclusters. Additionally, PIP3 nanoclusters and concomitant WAVE recruitment by GTP-loaded Rac1 (Oikawa et al., 2004; Lebensohn and Kirschner, 2009) further enhance nanoclusters' lifetime and nanocluster enrichment, which would consequently provide a positive feedback mechanism, sustaining cell migration.

EXPERIMENTAL PROCEDURES

Cell Culture

All single-molecule tracking, super-resolution experiments, and FRET biosensor imaging were performed on NIH 3T3 cells. Combined single-molecule tracking and optogenetics experiments were done with cos-7 cells. In

every case, cell culture was performed according to the American Type Culture Collection (ATCC) proposed protocol, cultured at 37°C in 5% CO₂ in DMEM and supplemented with 10% fetal calf serum. For single-molecule tracking and super-resolution experiments, we produced lentiviral stable cell lines expressing mEOS2-Rac1 mutants with a pHR backbone plasmid synthesized by Genescript. Cells were sorted using fluorescence-activated cell sorting. Optogenetics experiments were performed via triple transfection of CIBN-GFP (Valon et al., 2015), TIAM_linker_CRY2_IRFP obtained following the same routine as in (Valon et al., 2015), and mEOS2-Rac1 mutants using X-tremeGENE 9 and X-tremeGENE HP (Roche Applied Science, Penzberg, Bavaria, Germany) according to manufacturer's protocol. For drug treatment with the cocktail, cells were preincubated in 20 μM Y27632 for 10 min before the addition of 8 μM of jasplakinolide and 5 μM of latrunculin B. Movies were acquired ~7–12 min after the addition of jasplakinolide and latrunculin B. For the latrunculin B treatment alone, cells were incubated with 2 μM of latrunculin B, and movies were taken ~10–15 min after addition of the drug.

Cell Plating and Surface Patterning

For plating, cells were dissociated using Accutase (Life Technologies) and plated on 25 mm glass coverslips coated with fibronectin bovine protein (Life Technologies, Carlsbad, CA). Forty-nanometer-long crossbow fibronectin micro-patterned coverslips were fabricated following the protocol of Azioune et al. (2009) using PLL-g-PEG purchased from Surface Solutions Switzerland, a UV lamp (UV ozone oven 185 nm equipped with ozone catalyzer, UVO cleaner, model 342-220; Jelight), and a chrome mask (Toppan).

Single-Molecule Imaging

All experiments were imaged with a Metamorph (Molecular Devices, Eugene, OR) controlled IX71 Olympus inverted microscope, a 100× objective with NA 1.45 (Olympus, Melville, NY), and an ILAS2 azimuthal TIRF FRAP head (ilas2; Roper Scientific, Tucson, AZ) in an azimuthal TIRF configuration. Cells were kept at 37°C in 5% CO₂ with a heating chamber (Pecon; Meyer Instruments, Houston, TX). Single-molecule movies of the red form of mEOS2 were imaged at 40 ms with a 561 nm laser (Cobolt Jive 150; Hubner) of incident power of 2 kW/cm², and a BrightLine quad-edge beam splitter (Semrock Di01-R405/488/543/635). Photoconversion of mEOS2 was done with a 405 nm laser (Stradus 405; Vortran) in a TIRF configuration. Imaging of iRFP was done with a

642 nm laser (Stradus 642; Vortran) the same BrightLine dichroic, and a far-red emission filter (BLP01-635R-25; Semrock).

Analysis of Nanoclusters and Trajectories

We used the SLIMfast MATLAB code (Normanno et al., 2015) to recover single-molecule localizations and DBSCAN to identify nanoclusters. Trajectories were reconstructed by finding the optimal global assignment between points in consecutive frames using an inference approach. The mapping of diffusivities in single cells was achieved using a maximum likelihood approach. Single-cell maps were averaged using custom-built MATLAB routines. All these procedures are detailed in the [Supplemental Information](#).

Determination of Membrane Shuttling Rates

The shuttling rate of Rac1 to the membrane was analyzed using fluorescence recovery after photobleaching of the whole basal membrane of the green form of mEOS2 in TIRF mode, and recovery rates were determined as about 6 min and about 20 min (Figure S4) for spreading and spread cells, respectively.

Rac1 FRET Biosensors

We established a stable cell line of 3T3 cells expressing a Rac1-FRET-biosensor (Moshfegh et al., 2014). For imaging, cells were plated on glass coverslips with crossbow micropatterns. After 4 hr of adhesion, cells were imaged by epifluorescence using a Luca R camera (Andor on an Olympus IX71 microscope with a 60 \times magnification objective; Olympus PlanApo 60 \times , NA 1.45). The same excitation and dichroic mirrors (e.g., FF02-438/24, BS: FF-458-DiO2; Semrock) were used for the sequential acquisition of donor and acceptor images. A filter wheel was used to switch emission filters of donor (mCerulean, Em: FF01-483/32) and FRET acceptor (Em: FF01-542/27). Image processing included registration, flat-field correction, background subtraction, segmentation, and FRET/donor ratio calculations. FRET ratio images were then aligned and averaged as described in the [Supplemental Information](#).

Optogenetics

Recruitment of the catalytic domain of Tiam1 was performed using Cry2-CIBN light-gated dimerization as explained elsewhere (Valon et al., 2015). Localized recruitment was performed with 491 nm light, which is highly effective for optogenetic recruitment but less efficient for photoconversion of mEOS2. Recruitment laser pulses were applied every 10 s for 10 min. Single-molecule movies were obtained before and \sim 30 s after recruitment. The low 405 nm laser intensities used to photoconvert mEOS2 from the green to the red form did not introduce extensive global recruitment of Tiam1-Cry2-iRFP to the basal membrane. Imaging of iRFP was done with the same BrightLine dichroic and a far-red emission filter (BLP01-635R-25), and differential interference contrast (DIC) imaging was performed with a far-red filter in the illumination path to avoid CRY2 recruitment.

Immunofluorescence

Cell fixation and permeabilization were performed with 4% paraformaldehyde for 15 min and with 0.1% Triton X-100 or 0.5% NP40 for 5 min, respectively. To detect mouse WAVE2, a specific antibody called WP2 was raised against the peptide (C)NQRGSVLAGPKRRTS in rabbits. Specific antibodies from the rabbit serum were affinity-purified on a SulfoLink column (Pierce) displaying the same peptide. WP2 recognizes murine WAVE2 by western blot, immunofluorescence, and immunoprecipitates the WAVE complex. Anti-PIP3 was purchased from Echelon (Z-P345b) and used in a 1:100 concentration for 60 min. Goat anti-mouse and goat anti-rabbit Alexa Fluor 647-labeled secondary antibodies were purchased from Thermo Fisher Scientific (A-21236 and A-21245, respectively) and used in a 1:200 concentration for 60 min.

SUPPLEMENTAL INFORMATION

Supplemental Information includes Supplemental Experimental Procedures, six figures, and one movie and can be found with this article online at <https://doi.org/10.1016/j.celrep.2017.10.069>.

AUTHOR CONTRIBUTIONS

Conceptualization, A.R., M.D., and M.C.; Methodology, A.R., M.D., and M.C.; Software, A.R., J.-B.M., and M.C.; Formal Analysis, A.R. and M.C.; Investigation, A.R. and S.D.; Resources, F.C., F.D., G.C., and A.G.; Writing – Original Draft, A.R. and M.C.; Writing – Review & Editing, A.R., M.C., M.D., M.C.P., and A.G.; Visualization, A.R. and M.C.; Supervision, M.D. and M.C.; Funding Acquisition, M.D., M.C.P., and M.C.

ACKNOWLEDGMENTS

We thank Leo Valon for designing and making the TIAM_linker_CRY2_IRFP optogenetic plasmid. We thank Fred Etoc for the initial mEOS2-Rac1 construction and for preliminary experiments. M.C. acknowledges financial support from French National Research Agency (LICOP grant ANR-12-JSV5-0002-01). M.C. and M.D. acknowledge funding from French National Research Agency (ANR) Paris-Science-Lettres Program (grant ANR-10-IDEX-0001-02 PSL), Labex CelTisPhyBio (grant ANR-10-LBX-0038), and France-Biomedicine infrastructure supported by ANR grant ANR-10-INSB-04 (Investments for the Future). M.C. and M.C.P. acknowledge INSERM ITMO Plan Cancer 2014–2018 (PC201530).

Received: June 12, 2017

Revised: September 18, 2017

Accepted: October 18, 2017

Published: November 14, 2017

REFERENCES

- Azioune, A., Storch, M., Bornens, M., Théry, M., and Piel, M. (2009). Simple and rapid process for single cell micro-patterning. *Lab Chip* 9, 1640–1642.
- Bement, W.M., Miller, A.L., and von Dassow, G. (2006). Rho GTPase activity zones and transient contractile arrays. *BioEssays* 28, 983–993.
- Bieling, P., Li, T.D., Weichsel, J., McGorty, R., Jreij, P., Huang, B., Fletcher, D.A., and Mullins, R.D. (2016). Force feedback controls motor activity and mechanical properties of self-assembling branched actin networks. *Cell* 164, 115–127.
- Bisi, S., Disanza, A., Malinverno, C., Frittoli, E., Palamidessi, A., and Scita, G. (2013). Membrane and actin dynamics interplay at lamellipodia leading edge. *Curr. Opin. Cell Biol.* 25, 565–573.
- Blaževič, O., Mideksa, Y.G., Solman, M., Ligabue, A., Ariotti, N., Nakhaeizadeh, H., Fansa, E.K., Papageorgiou, A.C., Wittinghofer, A., Ahmadian, M.R., and Abankwa, D. (2016). Galectin-1 dimers can scaffold Raf-effectors to increase H-ras nanoclustering. *Sci. Rep.* 6, 24165.
- Bonny, M., Hui, X., Schweizer, J., Kaestner, L., Zeug, A., Kruse, K., and Lipp, P. (2016). C2-domain mediated nano-cluster formation increases calcium signaling efficiency. *Sci. Rep.* 6, 36028.
- Burkel, B.M., Benink, H.A., Vaughan, E.M., von Dassow, G., and Bement, W.M. (2012). A Rho GTPase signal treadmill backs a contractile array. *Dev. Cell* 23, 384–396.
- Castellana, M., Wilson, M.Z., Xu, Y., Joshi, P., Cristea, I.M., Rabinowitz, J.D., Gitai, Z., and Wingreen, N.S. (2014). Enzyme clustering accelerates processing of intermediates through metabolic channeling. *Nat. Biotechnol.* 32, 1011–1018.
- Cebecauer, M., Spitaler, M., Sergé, A., and Magee, A.I. (2010). Signalling complexes and clusters: functional advantages and methodological hurdles. *J. Cell Sci.* 123, 309–320.
- Chazeau, A., Mehidi, A., Nair, D., Gautier, J.J., Leduc, C., Chamma, I., Kage, F., Kechkar, A., Thoumine, O., Rottner, K., et al. (2014). Nanoscale segregation of actin nucleation and elongation factors determines dendritic spine protrusion. *EMBO J.* 33, 2745–2764.
- Das, S., Yin, T., Yang, Q., Zhang, J., Wu, Y.I., and Yu, J. (2015). Single-molecule tracking of small GTPase Rac1 uncovers spatial regulation of membrane translocation and mechanism for polarized signaling. *Proc. Natl. Acad. Sci. U S A* 112, E267–E276.

- Davis, M.J., Ha, B.H., Holman, E.C., Halaban, R., Schlessinger, J., and Boggon, T.J. (2013). RAC1P29S is a spontaneously activating cancer-associated GTPase. *Proc. Natl. Acad. Sci. U S A* *110*, 912–917.
- Duriscic, N., Laparra-Cuervo, L., Sandoval-Álvarez, A., Borbely, J.S., and Lakadamyali, M. (2014). Single-molecule evaluation of fluorescent protein photoactivation efficiency using an in vivo nanotemplate. *Nat. Methods* *11*, 156–162.
- Finkielstein, C.V., Overduin, M., and Capelluto, D.G.S. (2006). Cell migration and signaling specificity is determined by the phosphatidylserine recognition motif of Rac1. *J. Biol. Chem.* *281*, 27317–27326.
- Fricke, F., Beaudouin, J., Eils, R., and Heilemann, M. (2015). One, two or three? Probing the stoichiometry of membrane proteins by single-molecule localization microscopy. *Sci. Rep.* *5*, 14072.
- Fritz, R.D., and Pertz, O. (2016). The dynamics of spatio-temporal Rho GTPase signaling: formation of signaling patterns. *F1000Res* *5*, 749.
- García-Parajo, M.F., Cambi, A., Torreno-Pina, J.A., Thompson, N., and Jacobson, K. (2014). Nanoclustering as a dominant feature of plasma membrane organization. *J. Cell Sci.* *127*, 4995–5005.
- Gautier, J.J., Lomakina, M.E., Bouslama-Oueghlani, L., Derivery, E., Beilinson, H., Faigle, W., Loew, D., Louvard, D., Echard, A., Alexandrova, A.Y., et al. (2011). Clathrin is required for Scar/Wave-mediated lamellipodium formation. *J. Cell Sci.* *124*, 3414–3427.
- Gc, J.B., Gerstman, B.S., Stahelin, R.V., and Chapagain, P.P. (2016). The Ebola virus protein VP40 hexamer enhances the clustering of PI(4,5)P 2 lipids in the plasma membrane. *Phys. Chem. Chem. Phys.* *18*, 7–9.
- Groves, J.T., and Kuriyan, J. (2010). Molecular mechanisms in signal transduction at the membrane. *Nat. Struct. Mol. Biol.* *17*, 659–665.
- Hancock, J.F., and Parton, R.G. (2005). Ras plasma membrane signalling platforms. *Biochem. J.* *389*, 1–11.
- Harding, A.S., and Hancock, J.F. (2008). Using plasma membrane nanoclusters to build better signaling circuits. *Trends Cell Biol.* *18*, 364–371.
- Haugh, J.M., Codazzi, F., Teruel, M., and Meyer, T. (2000). Spatial sensing in fibroblasts mediated by 3' phosphoinositides. *J. Cell Biol.* *151*, 1269–1280.
- Heo, W.D., Inoue, T., Park, W.S., Kim, M.L., Park, B.O., Wandless, T.J., and Meyer, T. (2006). PI(3,4,5)P3 and PI(4,5)P2 lipids target proteins with polybasic clusters to the plasma membrane. *Science* *314*, 1458–1461.
- Hobbs, G.A., Wittinghofer, A., and Der, C.J. (2016). Selective targeting of the KRAS G12C mutant: kicking KRAS when it's down. *Cancer Cell* *29*, 251–253.
- Hodgson, L., Spiering, D., Sabouri-Ghomi, M., Dagliyan, O., DerMardirossian, C., Danuser, G., and Hahn, K.M. (2016). FRET binding antenna reports spatio-temporal dynamics of GDI-Cdc42 GTPase interactions. *Nat. Chem. Biol.* *12*, 802–809.
- Honigsmann, A., van den Bogaart, G., Iraheta, E., Risselada, H.J., Milovanovic, D., Mueller, V., Müller, S., Diederichsen, U., Fasshauer, D., Grubmüller, H., et al. (2013). Phosphatidylinositol 4,5-bisphosphate clusters act as molecular beacons for vesicle recruitment. *Nat. Struct. Mol. Biol.* *20*, 679–686.
- Huang, C.-H., Tang, M., Shi, C., Iglesias, P.A., and Devreotes, P.N. (2013). An excitable signal integrator couples to an idling cytoskeletal oscillator to drive cell migration. *Nat. Cell Biol.* *15*, 1307–1316.
- Iyengar, G., and Rao, M. (2014). A cellular solution to an information-processing problem. *Proc. Natl. Acad. Sci. U S A* *111*, 12402–12407.
- Ji, C., Zhang, Y., Xu, P., Xu, T., and Lou, X. (2015). Nanoscale landscape of phosphoinositides revealed by specific pleckstrin homology (PH) domains using single-molecule superresolution imaging in the plasma membrane. *J. Biol. Chem.* *290*, 26978–26993.
- Johnson, J.L., Erickson, J.W., and Cerione, R.A. (2012). C-terminal di-arginine motif of Cdc42 protein is essential for binding to phosphatidylinositol 4,5-bisphosphate-containing membranes and inducing cellular transformation. *J. Biol. Chem.* *287*, 5764–5774.
- Kennedy, M.J., Hughes, R.M., Peteya, L.A., Schwartz, J.W., Ehlers, M.D., and Tucker, C.L. (2010). Rapid blue-light-mediated induction of protein interactions in living cells. *Nat. Methods* *7*, 973–975.
- Kholodenko, B.N., Hancock, J.F., and Kolch, W. (2010). Signalling ballet in space and time. *Nat. Rev. Mol. Cell Biol.* *11*, 414–426.
- Köster, D.V., Husain, K., Iljazi, E., Bhat, A., Bieling, P., Mullins, R.D., Rao, M., and Mayor, S. (2016). Actomyosin dynamics drive local membrane component organization in an in vitro active composite layer. *Proc. Natl. Acad. Sci. U S A* *113*, E1645–E1654.
- Krause, M., and Gautreau, A. (2014). Steering cell migration: lamellipodium dynamics and the regulation of directional persistence. *Nat. Rev. Mol. Cell Biol.* *15*, 577–590.
- Lawson, C.D., and Burridge, K. (2014). The on-off relationship of Rho and Rac during integrin-mediated adhesion and cell migration. *Small GTPases* *5*, e27958.
- Lebensohn, A.M., and Kirschner, M.W. (2009). Activation of the WAVE complex by coincident signals controls actin assembly. *Mol. Cell* *36*, 512–524.
- Li, L., Shi, X., Guo, X., Li, H., and Xu, C. (2014). Ionic protein-lipid interaction at the plasma membrane: what can the charge do? *Trends Biochem. Sci.* *39*, 130–140.
- Machacek, M., Hodgson, L., Welch, C., Elliott, H., Pertz, O., Nalbant, P., Abell, A., Johnson, G.L., Hahn, K.M., and Danuser, G. (2009). Coordination of Rho GTPase activities during cell protrusion. *Nature* *461*, 99–103.
- Manley, S., Gillette, J.M., Patterson, G.H., Shroff, H., Hess, H.F., Betzig, E., and Lippincott-Schwartz, J. (2008). High-density mapping of single-molecule trajectories with photoactivated localization microscopy. *Nat. Methods* *5*, 155–157.
- Mendoza, M.C., Vilela, M., Juárez, J.E., Blenis, J., and Danuser, G. (2015). ERK reinforces actin polymerization to power persistent edge protrusion during motility. *Sci. Signal.* *8*, ra47.
- Moshfegh, Y., Bravo-Cordero, J.J., Miskolci, V., Condeelis, J., and Hodgson, L. (2014). A Trio-Rac1-Pak1 signalling axis drives invadopodia disassembly. *Nat. Cell Biol.* *16*, 574–586.
- Navarro-Lérida, I., Sánchez-Perales, S., Calvo, M., Rentero, C., Zheng, Y., Enrich, C., and Del Pozo, M.A. (2012). A palmitoylation switch mechanism regulates Rac1 function and membrane organization. *EMBO J.* *31*, 534–551.
- Normanno, D., Boudarène, L., Dugast-Darzacq, C., Chen, J., Richter, C., Proux, F., Bénichou, O., Voituriez, R., Darzacq, X., and Dahan, M. (2015). Probing the target search of DNA-binding proteins in mammalian cells using TetR as model searcher. *Nat. Commun.* *6*, 7357.
- Oikawa, T., Yamaguchi, H., Itoh, T., Kato, M., Ijuin, T., Yamazaki, D., Suetsugu, S., and Takenawa, T. (2004). PtdIns(3,4,5)P3 binding is necessary for WAVE2-induced formation of lamellipodia. *Nat. Cell Biol.* *6*, 420–426.
- Parrini, M.C., Sadou-Dubourgoux, A., Aoki, K., Kunida, K., Biondini, M., Hatzoglou, A., Pouillet, P., Formstecher, E., Yeaman, C., Matsuda, M., et al. (2011). SH3BP1, an exocyst-associated RhoGAP, inactivates Rac1 at the front to drive cell motility. *Mol. Cell* *42*, 650–661.
- Peng, G.E., Wilson, S.R., and Weiner, O.D. (2011). A pharmacological cocktail for arresting actin dynamics in living cells. *Mol. Biol. Cell* *22*, 3986–3994.
- Pertz, O. (2010). Spatio-temporal Rho GTPase signaling—where are we now? *J. Cell Sci.* *123*, 1841–1850.
- Petrie, R.J., Doyle, A.D., and Yamada, K.M. (2009). Random versus directionally persistent cell migration. *Nat. Rev. Mol. Cell Biol.* *10*, 538–549.
- Pezzarossa, A., Zosel, F., and Schmidt, T. (2015). Visualization of HRas domains in the plasma membrane of fibroblasts. *Biophys. J.* *108*, 1870–1877.
- Picas, L., Gaits-Iacovoni, F., and Goud, B. (2016). The emerging role of phosphoinositide clustering in intracellular trafficking and signal transduction. *F1000Res* *5*, 422.
- Plowman, S.J., Muncke, C., Parton, R.G., and Hancock, J.F. (2005). H-ras, K-ras, and inner plasma membrane raft proteins operate in nanoclusters with differential dependence on the actin cytoskeleton. *Proc. Natl. Acad. Sci. U S A* *102*, 15500–15505.
- Raghupathy, R., Anilkumar, A.A., Polley, A., Singh, P.P., Yadav, M., Johnson, C., Suryawanshi, S., Saikam, V., Sawant, S.D., Panda, A., et al. (2015).

- Transbilayer lipid interactions mediate nanoclustering of lipid-anchored proteins. *Cell* 161, 581–594.
- Roob, E., 3rd, Trendel, N., Rein Ten Wolde, P., and Mugler, A. (2016). Cooperative clustering digitizes biochemical signaling and enhances its fidelity. *Biophys. J.* 110, 1661–1669.
- Rossier, O., Ochteau, V., Sibarita, J.B., Leduc, C., Tessier, B., Nair, D., Gatterdam, V., Destaing, O., Albigès-Rizo, C., Tampé, R., et al. (2012). Integrins $\beta 1$ and $\beta 3$ exhibit distinct dynamic nanoscale organizations inside focal adhesions. *Nat. Cell Biol.* 14, 1057–1067.
- Salamon, R.S., and Backer, J.M. (2013). Phosphatidylinositol-3,4,5-trisphosphate: tool of choice for class I PI 3-kinases. *BioEssays* 35, 602–611.
- Schütz, G.J., Schindler, H., and Schmidt, T. (1997). Single-molecule microscopy on model membranes reveals anomalous diffusion. *Biophys. J.* 73, 1073–1080.
- Schwartz, M.A. (1997). Integrins, oncogenes, and anchorage independence. *J. Cell Biol.* 139, 575–578.
- Shibata, A.C.E., Chen, L.H., Nagai, R., Ishidate, F., Chadda, R., Miwa, Y., Naruse, K., Shirai, Y.M., Fujiwara, T.K., and Kusumi, A. (2013). Rac1 recruitment to the archipelago structure of the focal adhesion through the fluid membrane as revealed by single-molecule analysis. *Cytoskeleton (Hoboken)* 70, 161–177.
- Shivanandan, A., Unnikrishnan, J., and Radenovic, A. (2015). On characterizing membrane protein clusters with model-free spatial correlation approaches. *bioRxiv*. <https://doi.org/10.1101/030718>.
- Specht, C.G., Grünewald, N., Pascual, O., Rostgaard, N., Schwarz, G., and Triller, A. (2011). Regulation of glycine receptor diffusion properties and gephyrin interactions by protein kinase C. *EMBO J.* 30, 3842–3853.
- Stahelin, R.V., Scott, J.L., and Frick, C.T. (2014). Cellular and molecular interactions of phosphoinositides and peripheral proteins. *Chem. Phys. Lipids* 182, 3–18.
- Théry, M., Racine, V., Piel, M., Pépin, A., Dimitrov, A., Chen, Y., Sibarita, J.B., and Bornens, M. (2006). Anisotropy of cell adhesive microenvironment governs cell internal organization and orientation of polarity. *Proc. Natl. Acad. Sci. U S A* 103, 19771–19776.
- Tian, T., Harding, A., Inder, K., Plowman, S., Parton, R.G., and Hancock, J.F. (2007). Plasma membrane nanoswitches generate high-fidelity Ras signal transduction. *Nat. Cell Biol.* 9, 905–914.
- Tran, T.N., Drab, K., and Daszykowski, M. (2013). Revised DBSCAN algorithm to cluster data with dense adjacent clusters. *Chemometr. Intell. Lab. Syst.* 120, 92–96.
- Um, K., Niu, S., Duman, J.G., Cheng, J.X., Tu, Y.K., Schwechter, B., Liu, F., Hiles, L., Narayanan, A.S., Ash, R.T., et al. (2014). Dynamic control of excitatory synapse development by a Rac1 GEF/GAP regulatory complex. *Dev. Cell* 29, 701–715.
- Valon, L., Etoc, F., Remorino, A., di Pietro, F., Morin, X., Dahan, M., and Coppey, M. (2015). Predictive spatiotemporal manipulation of signaling perturbations using optogenetics. *Biophys. J.* 109, 1785–1797.
- van den Bogaart, G., Meyenberg, K., Risselada, H.J., Amin, H., Willig, K.I., Hubrich, B.E., Dier, M., Hell, S.W., Grubmüller, H., Diederichsen, U., and Jahn, R. (2011). Membrane protein sequestering by ionic protein-lipid interactions. *Nature* 479, 552–555.
- Veatch, S.L., Machta, B.B., Shelby, S.A., Chiang, E.N., Holowka, D.A., and Baird, B.A. (2012). Correlation functions quantify super-resolution images and estimate apparent clustering due to over-counting. *PLoS ONE* 7, e31457.
- Viaud, J., Lagarrigue, F., Ramel, D., Allart, S., Chicanne, G., Ceccato, L., Courilleau, D., Xuereb, J.M., Pertz, O., Payrastra, B., and Gaits-Iacovoni, F. (2014). Phosphatidylinositol 5-phosphate regulates invasion through binding and activation of Tiam1. *Nat. Commun.* 5, 4080.
- Wang, J., and Richards, D.A. (2012). Segregation of PIP2 and PIP3 into distinct nanoscale regions within the plasma membrane. *Biol. Open* 1, 857–862.
- Wang, S., Watanabe, T., Matsuzawa, K., Katsumi, A., Kakeno, M., Matsui, T., Ye, F., Sato, K., Murase, K., Sugiyama, I., et al. (2012). Tiam1 interaction with the PAR complex promotes talin-mediated Rac1 activation during polarized cell migration. *J. Cell Biol.* 199, 331–345.
- Weiger, M.C., Wang, C.C., Krajcovic, M., Melvin, A.T., Rhoden, J.J., and Haugh, J.M. (2009). Spontaneous phosphoinositide 3-kinase signaling dynamics drive spreading and random migration of fibroblasts. *J. Cell Sci.* 122, 313–323.
- Wertheimer, E., Gutierrez-Uzquiza, A., Roseblit, C., Lopez-Haber, C., Sosa, M.S., and Kazanietz, M.G. (2012). Rac signaling in breast cancer: a tale of GEFs and GAPs. *Cell. Signal.* 24, 353–362.
- Wittinghofer, A., ed. (2014). *Ras Superfamily Small G Proteins: Biology and Mechanisms 1* (Springer). <https://doi.org/10.1007/978-3-7091-1806-1>. <http://www.springer.com/us/book/9783709118054>.
- Woods, B., Kuo, C.C., Wu, C.F., Zyla, T.R., and Lew, D.J. (2015). Polarity establishment requires localized activation of Cdc42. *J. Cell Biol.* 211, 19–26.
- Yang, H.W., Collins, S., and Meyer, T. (2016). Locally excitable Cdc42 signals steer cells during chemotaxis. *Nat. Cell Biol.* 18, 191–201.
- Zhang, B., Gao, Y., Moon, S.Y., Zhang, Y., and Zheng, Y. (2001). Oligomerization of Rac1 gtpase mediated by the carboxyl-terminal polybasic domain. *J. Biol. Chem.* 276, 8958–8967.
- Zhou, Y., and Hancock, J.F. (2015). Ras nanoclusters: versatile lipid-based signaling platforms. *Biochim. Biophys. Acta Mol. Cell Res.* 1853, 841–849.